The Eurasia Proceedings of Science, Technology, Engineering & Mathematics (EPSTEM)
ISSN: 2602-3199

The Eurasia Proceedings of Science, Technology, Engineering & Mathematics (EPSTEM), 2024

Volume 28, Pages 565-574

ICBASET 2024: International Conference on Basic Sciences, Engineering and Technology

Optimization of Properties of Iron Oxide Nanoparticles Synthized by Sol-Gel Method

Gulten Sadullahoglu
Istanbul Health and Technology University

Abstract: In this study, the effects of pH value and capping agent on the morphology, pore structure and size of iron oxide nanoparticles were investigated systematically to obtain optimum properties. Iron oxide nanoparticles were synthized by sol-gel method. Polyvinyl alcohol (PVA) was used as capping agent by adding to the solution at 70 °C. After the drying process the powders were heat treated at 250 °C for 2 h under air atmosphere. Particle size of each sample was determined by using ZetaSizer instrument. X-ray diffraction (XRD) technique was employed for structural properties of iron oxide nanoparticles, FE-SEM (Field Emmision Scanning Electron Microscopy) was used to analyze the morphology of the powders. Magnetic properties of the nanoparticles were measured by VSM (Vibrating Sample Magnetometer) under air atmosphere at room temperature. Spesific surface area, porosity and pore size distribution of iron oxide nanoparticles were calculated by Brunauer-Emmett-Teller (BET) instrument. The results indicated that formation of the γ-Fe_2O_3 is sensitive to either the pH value of the solution or the capping agent, for the uncoated samples when pH value of the solution is adjusted to 2.5, α-Fe_2O_3 phase was detected as a single phase. When the solution was neutralized, γ-Fe_2O_3 was formed as the major phase in the microstructure, γ-Fe_2O_3 phase was formed as the major phase in the PVA coated samples leading to highest value of 50.33 emu/g measured in the sample of PVA8.5. For the PVA coated samples, specific surface area is in the range of 15.73 – 20.81 m^2/g, the intervals of pore volume and average pore width are increased to 0.099 – 0.121 cm^3/g and 23.19 – 23.07 nm respectively.

Keywords: Magnetic nanoparticles, Sol–Gel method, Capping agent, Pore structure, X-Ray diffraction

Introduction

Because of their chemical stability, cheap, and non-toxic nature iron oxide nanoparticles have attracted tremendous interest from researchers. Iron oxide, in nature has many phases like α-Fe_2O_3, β-Fe_2O_3, γ-Fe_2O_3, and Fe_3O_4. Out of all these polymorphic forms, α-Fe_2O_3 nanoparticles are most stable at ambient conditions (Ramasami et al., 2023). α-Fe_2O_3 nanoparticle is more popular than others due to its cost-effective synthesis, non-toxic nature, stability at room temperature, environment friendliness, a reusable and a wide range of applications such as catalysts, contrast agents in Magnetic Resonance Imaging (MRI), anticancer therapeutics (Behera et al., 2020; Ghosh et al., 2020; Rasheed et al., 2018;), drug delivery, pigments, gas sensors and biosensors (Guardia et al., 2000; Katsuki & Komarneni, 2003; Tedeschi & Enders, 2001). Different methods have been reported for the synthesis of iron oxide nanoparticles that includes, hydrothermal, co-precipitation, microemulsion, thermal decomposition, green synthesis, sol-gel, high-energy ball milling, etc, (Bhavani et al., 2017; Bhuiyan et al., 2020; Gonzalez-Moragas et al., 2015; LaGrow et al., 2019; Lemine et al., 2010; Okoli et al., 2012; Ravikumar & Bandyopadhyaya, 2011; Woo et al., 2003). But there are some challenges in controlling the particle size, shape, monodispersity, and morphology due to the high surface energy of iron oxide nanoparticles leading to aggregation under normal reaction condition (Jain et al., 2005; Mahmoudi et al., 2010; Mornet et al., 2005). To overcome these limitations scientists have applied different annealing temperature, reaction pH and capping agents (Woo et al., 2003; Predescu et al., 2018; Sharma, et al., 2019; Kumari et al., 2018; Sharma et al., 2021).

A. Bandhu at. Reported that when molarity of citric acid was between 0.05 and 0.2 M and at 400 °C annealing temperature α-Fe_2O_3 and γ-Fe_2O_3 phases were detected in XRD analysis however, at 210 °C, only α-Fe_2O_3 was observed and particle size changed from 22 nm to 56 nm when citric acid concentration decreased to 0.05 M in the solution. When some chemicals were added to the solution in stead of citric acid pore structure changed considerably and γ-Fe_2O_3 phase was formed in the structure. When iron oxide nanoparticles were coated with pepsin, high saturation magnetization was obtained as magnetic biomaterial for magnetically controlled drug delivery (Bandhu et al., 2015). Capping agents have clinical a significance to produce biocompatible nanoparticles. The covalent bonding between the chains of capping ligands and the nanoparticles' surface leads to steric hindrance providing stability to the nanocomposite (Javed et al., 2020). In this study, to investigate the effects of pH value of solution and application of Polyvinyl Alcohol (PVA) as capping acent on particle size, pore structure, magnetic properties, phase formation and microstructure to reach optimum properties.

Experimantal

All chemicals including iron nitrate nonahydrate ($Fe(NO_3)_3.9H_2O$), citric acid ($C_6H_8O_7$), polyvinylalcohol (PVA), were obtained from Merck and used as received, without further purification. Uncoated and PVA coated samples were prepared by the sol–gel method. $Fe(NO_3)_3.9H_2O$ was disolved in distilled water by using magnetic stirrer at 400 rpm. Citric acid ($C_6H_8O_7$) was added to the solution with molar ratio of citrate to nitrate 1:1. pH value of the solution are adjusted as 2.5, 7, 8.5 and 10 by adding NH_4OH dropwise to the solution. The mixture was simultaneously mixed and heated at 70 °C, when gel was obtained samples were dried at gradually increasing temperatures from 135 °C to 185 °C 135. Dried powders were heat treated at 250 ° for 2 h under air atmosphere. For the production of the coated samples, Polyvinyl alcohol (PVA) was added to the solution slowly over about 45 minutes while the precursers were mixed in a magnetic stirrer, Fe:PVA ratio is 1:1, followed by the same procedure as for the uncoated sample.

X-ray diffraction patterns of all the samples were recorded in powder X-ray diffractometer, Malvern PANalytical X'Pert PRO model, using Cu Kα radiation (α = 0.15425 nm) in the range of 2θ from 3° to 90°. The microstructure of the samples was observed by field-emission scanning electron microscopy by Thermo Scientific Apreo 2 S LoVac. Surface area, porosity and adsorption capacity are measured using the Brunauer, Emmett and Teller (BET) method in a 77 K liquid nitrogen environment, based on nitrogen (N_2). Particle size of the samples were measured by Malvern Nano ZS. Magnetic properties of the samples were measured at room temperature between -10000 - +10000 Oe external magnetic field by using Dexing Magnet VSM 550.

Results and Discussion

XRD Analysis

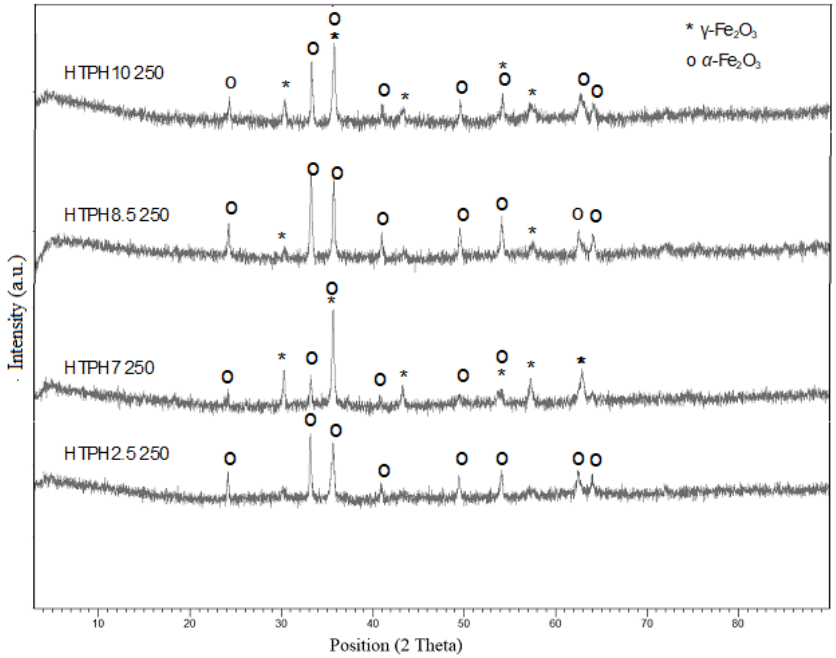

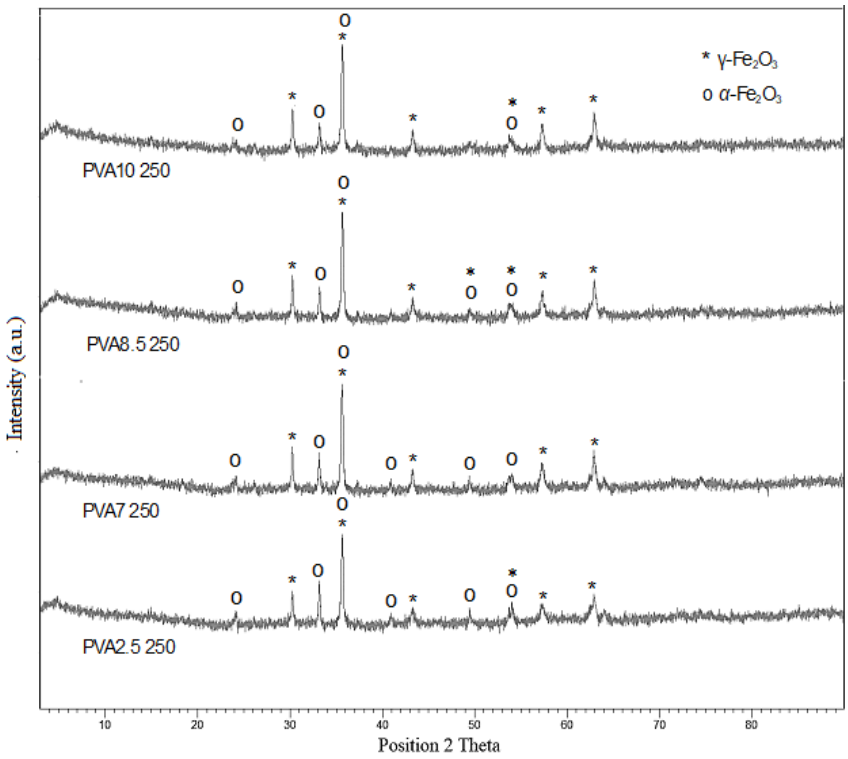

Figure 1. XRD patterns of the uncoated and PVA coated samples.

Figure 1 shows the diffraction patterns of the samples, for the sample of HTPH2.5 diffraction peaks detected belongs to α-Fe_2O_3 (hematite) phase. in the material. Diffraction peaks of α-Fe_2O_3 were found at 24.13° , 33.13° , 35.59° , 40.85° , 49.43°, 54.05°, 62.47° and 63.79° of 2θ and were correlated with Miller indices of (0 1 2), (1 0 4), (1 1 0), (1 1 3), (0 2 4), (1 1 6), (2 1 4) and (3 0 0) having ICSD file No. 89-2810.

When the pH value of the solution for the uncoated sample was increased to 7, the diffraction peaks corresponding to ferromagnetic γ-Fe_2O_3 phase were detected as a major phase Diffraction peaks of γ-Fe_2O_3 were found at 30.24° , 35.6° , 43.25° , 53.82° , 57.27° and 62.85° of 2θ and were correlated with Miller indices of (2 2 0), (3 1 1), (4 0 0), (2 1 1), (5 1 1) and (4 4 0) respectively having ICSD file No. 39-1346.

SEM Analysis

The micrographs of the uncoated and PVA coated samples are presented in Figure 1. In the SEM microstructure images of coated and uncoated samples, nanoparticles are of different shapes and sizes, and it has been observed that these particles form aggregates. mesoporous structure between in stuck nanoparticles provides a hysteresis in adsorption and desorption isotherm. In Figure 2(g)-(h), PVA coated samples show a distribution of spherical nanoparticles which were stuck together.

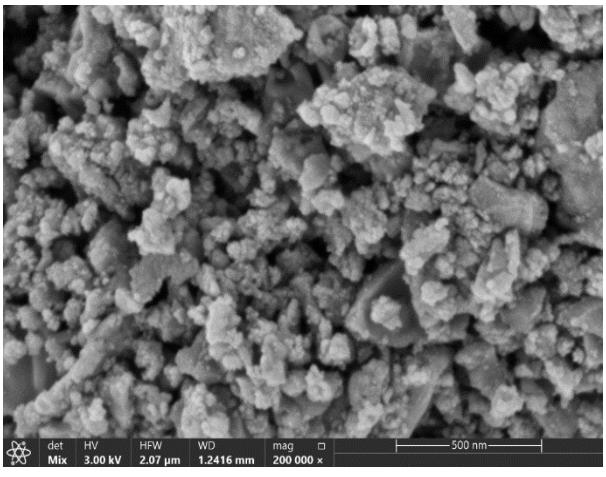

(a)

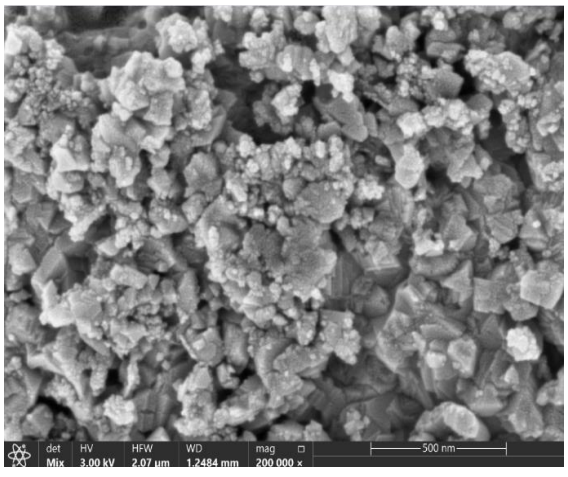

(b)

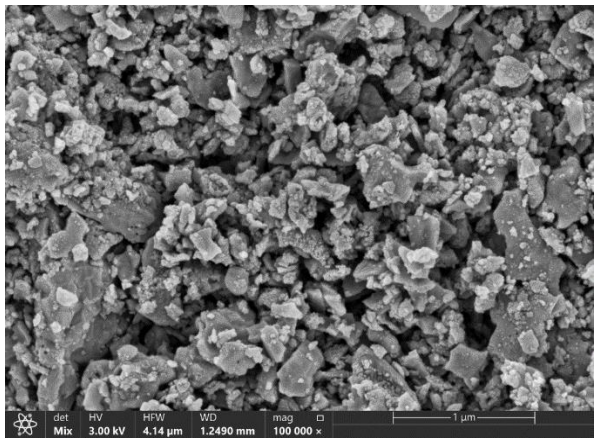

(c)

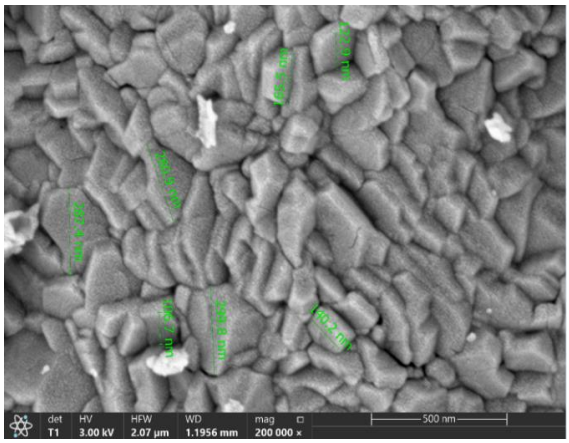

(d)

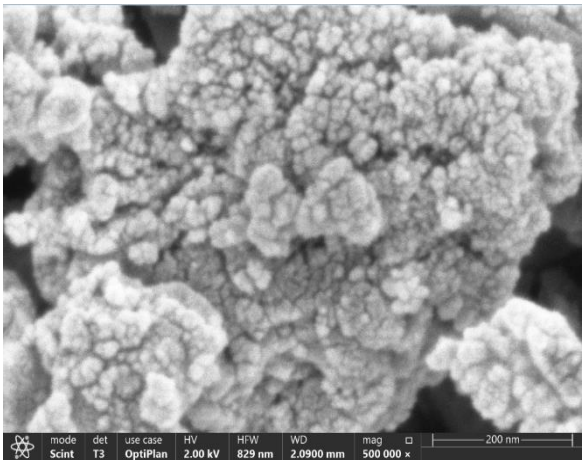

(e)

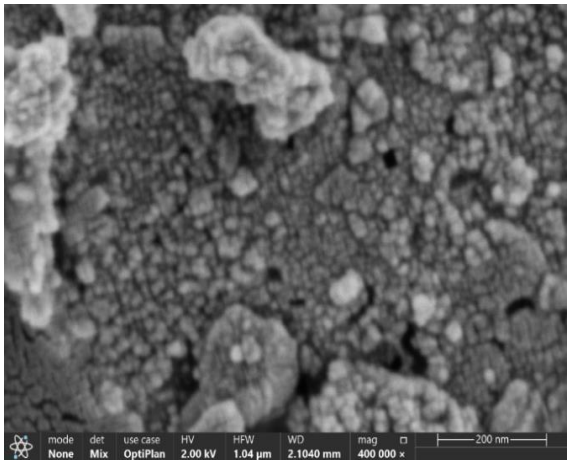

(f)

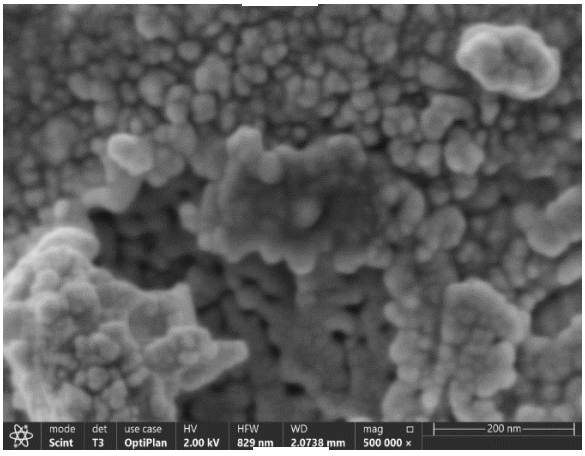

(g)

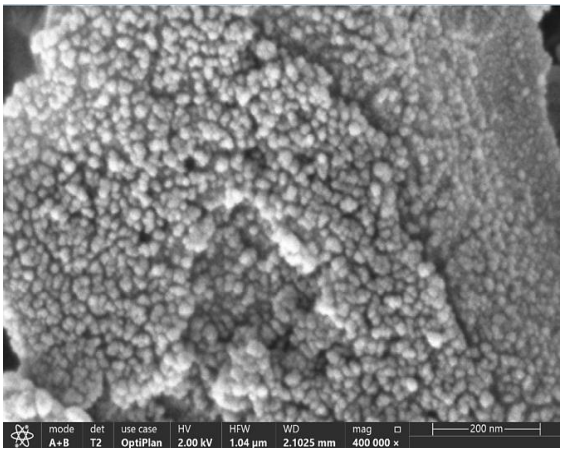

(h)

Figure 2. HRSEM images of the uncoated (a -d) and PVA coated (e -h) samples.

Nitrogen Gas Adsorption Analysis

Structure of Fe_2O_3 Samples were Determined by BET Analysis

The low-temperature liquid nitrogen adsorption experiment includes the adsorption/desorption curve and pore size change. The experimental results of the samples are compared with the results of samples which have

processed at different pH value and the coated samples to obtain the effect of nanoparticle adsorption on the pore structure (Table 2).

Figure 1. shows the adsorbtion and desorption isotherms of the samples. Adsorption/desorption curves are determined by the Barrett–Joyner Halenda (BJH) method through analyzing the desorption branch of adsorption data. It can be seen from the curves of the coated and uncoated samples that the adsorption curves belong to type III isotherms are concave, and the amount of adsorbed gas increases with the increase of the component relative pressure.

In such cases, the adsorbent—adsorbate interaction is weak as compared with the adsorbate—adsorbate interactions.The hysteresis loops of the samples belong to H3 hysteresis loops. Type H3 loop, which does not exhibit any limiting adsorption at high relative pressure is observed with aggregates of plate-like particles giving rise to slit-shaped pores. Also if the pore network consists of macropores which are not completely filled with pore condensate (Wang et al., 2022).

In Figure 2 (a), (b) and (d) desoption isotherms have steep clousers at about 0,4 relative pressure this is due to the cavitation – induced evoporation. In the case of the sample HTP8,5 and all the coated samples (Figure (c), (e)-(h)) desorption isotherms of changes smoothly when the relative pressure decreases in the removing of adsorbate process. This may referred that adsorbate molecules can be desorbed easer from pores than that of other samples.

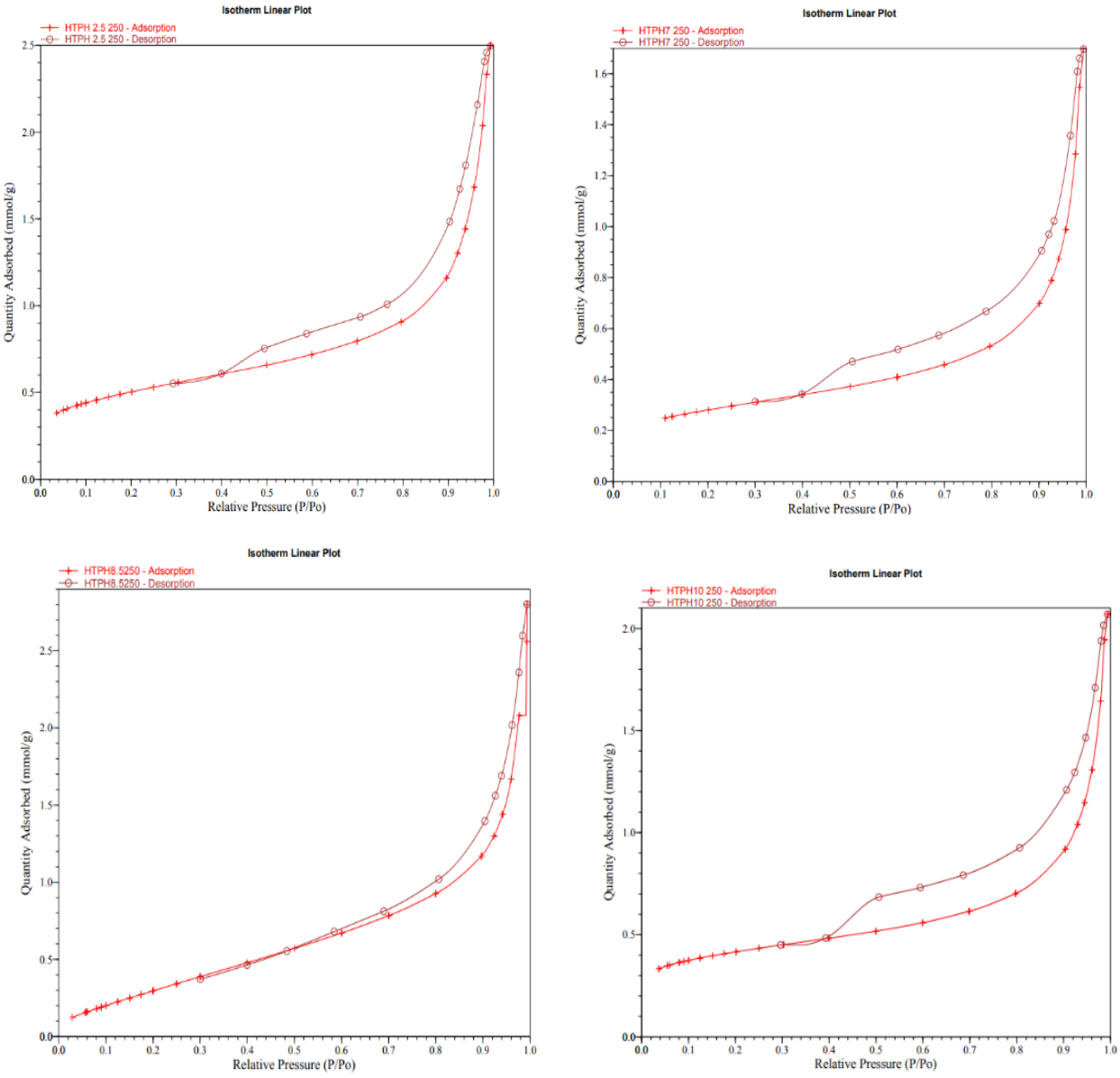

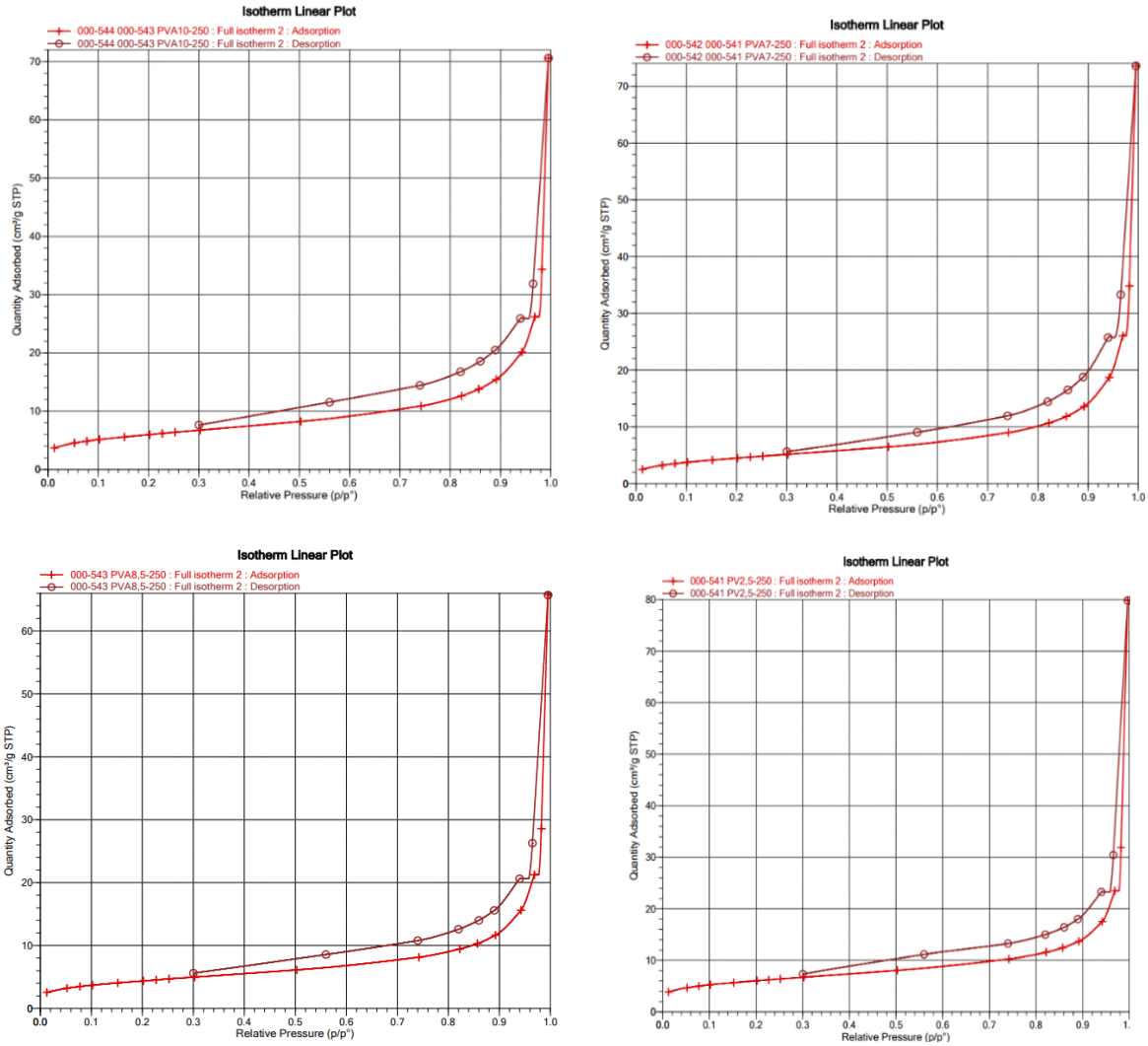

Figure 3. Adsorption and desorption isotherms of the uncoated and PVA coated nanoparticles**.**

The average pore diameter and specific surface data in Table 2 are determined by the Brunauer–Emmett–Teller (BET) method in the low-temperature liquid nitrogen adsorption experiment.The specific surface area, pore volumes and average pore diameters of the uncoated iron oxide samples varied between 22.2-40.1 m^2 /g, 0.055-0.097 cm^3 /g and 9.536-13.873 nm, respectively.

Table 1. Surface area (m^2/g), pore volume (cm^3/g), average pore diameter (nm) and particle size (nm) of the uncoated and PVA coated samples.

Sample	Surface Area (m^2/g)	Pore Volume (cm^3/g)	Average Pore Diameter (nm)
HTPH2.5250	40.1075	0.0827	9.53620
HTPH7250	22.2038	0.0556	13.8736
HTPH8.5250	28.4509	0.0973	9.4389
HTPH10250	32.6688	0.0667	11.2474
PVA2.5250	20,8158	0,1209	29,0750
PVA7250	15,7323	0,1123	27,4403
PVA8.5250	15,7747	0,0999	28,0846
PVA10250	20,7509	0,1069	23,1963

In the case of the samples capped with PVA, the pore volume of the samples were significantly increased and the spesific surface area of the PVA coated samples were lower than the uncoated samples. The specific surface area, pore volumes and average pore diameter of the PVA coated samples between 15.73-20.81 m^2 /g, 0.0999-0.1209 cm^3 /g and 23.196-29.075 nm, respectively.

Particle Size Measurements

The average particle size is between 1166 nm and 1473 nm for uncoated samples, a homogeneous distribution in the microstructure was observed only for the HTP2.5 sample. Different size distributions are observed in PVA coated samples, the average particle size is between 1066 nm and 1711 nm.

Figure 4. Particle size measurements of the uncoated and PVA coated samples.

Magnetic Properties

The effect of pH value of solution and PVA coating on the magnetic properties has been studied at room temperature. Figure 5 highlights the magnetization measurements as a function of the applied external magnetic field. Various magnetic parameters such as saturation magnetization (M_S), remanent magnetization (M_R), and

coercivity (H_c) have been evaluated using the M − H loops and are shown in Table 2. For the uncoated samples, the saturation of magnetization calculated using the M − H loop was found between 13.75 - 44.85 emu/g (Table 2).

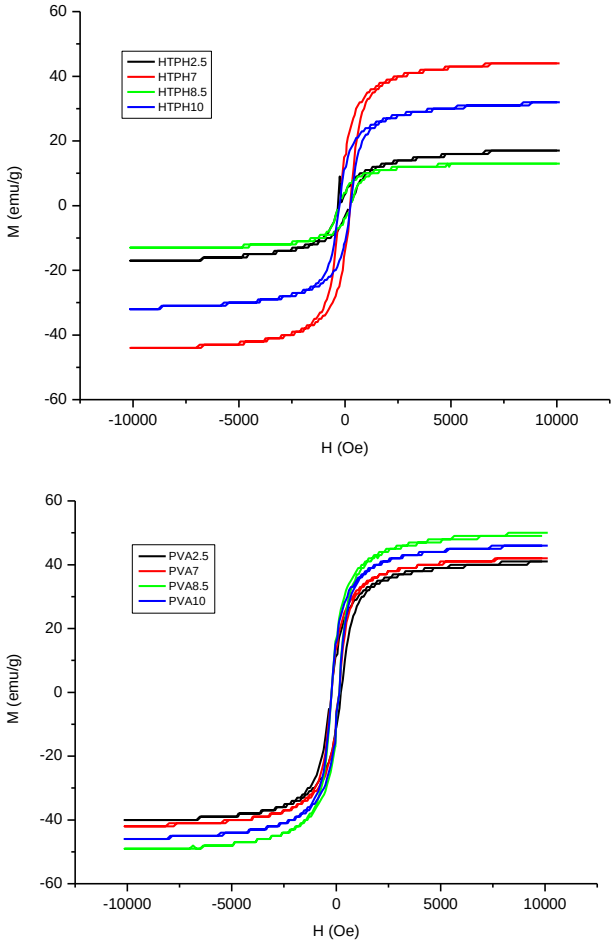

Figure 5. Hysteresis loops of the uncoated and PVA coated samples.

The magnetization of the samples increased on the formation of ferrimagnetic γ-Fe_2O_3 phase in the microstructure depending on the pHvalue of the solution fort he uncoated samples.

Table 2. Magnetic properties of the uncoated and PVA coated samples.

Sample	**M_s (emu/g)**	**M_R (emu/g)**	**H_c (Oe)**
HTPH-2.5	18.89	4.08	250.70
HTPH-7	44.85	15.94	247.65
HTPH-8.5	13.75	4.65	250.70
HTPH-10	32.33	11.91	267.05
PVA-2.5	41.60	12.05	239.06
PVA-7	42.46	14.04	224.22
PVA-8.5	50.33	17.39	226.72
PVA-10	46.61	15.85	219.96

PVA coated samples have higher saturation magnetization values between 41.60 – 50.33 emu/g, because ferrimagnetic γ-Fe_2O_3 phase was detected as major phase in the XRD diffraction patterns.

Conclusions

In this study, iron oxide nanoparticles have been produced by sol-gel method, in the X-Ray diffraction patterns ofthe samples, for the uncoated samples when pH value of the solution is adjusted to 2.5, α-Fe_2O_3 phase was detected as a single phase. When the solution was neutralized, γ-Fe_2O_3 was formed as the major phase in the

microstructure for the further increament of pH value, γ-Fe_2O_3 was formed as the secondary phase. In PVA coated samples, the γ-Fe_2O_3 phase was formed as the major phase. In this case, it can be concluded that the formation of the γ-Fe_2O_3 is sensitive to either the pH value of the solution or the capping agent.

The existence of ferromagnetic γ-Fe_2O_3 phase in the materials caused the M_s value to reach the highest value of 44.85 emu/g for the uncoated samples. This value increased to 50.33 emu/g measured in the sample of PVA8.5. For the uncoated samples, BET measurement indicated that specific surfase area, pore volume and average pore width are in the range of 40.10 – 32.2 m^2/g, 0.082 – 0.056 cm^3/g and 9.43 – 13.87 nm respectively. In the adsorption and desoption isotherms, desorption curves have steep clousers at about 0.4 relative pressure except for the sample HTPH8.5. Because pores are larger and open ended in the particles which causes adsorbate molecules to be desorbed easily from pores.

For the PVA coated samples, specific surface area is in the range of 15.73 – 20.81 m^2/g, the intervals of pore volume and average pore width are increased to 0.099 – 0.121 cm^3/g and 23.19 – 23.07 nm respectively. In the drug delivery, increase in pore volume provides carrying more drug in the particles.

Scientific Ethics Declaration

The author declares that the scientific ethical and legal responsibility of this article published in EPSTEM journal belongs to the author.

Acknowledgements or Notes

* This article was presented as an oral presentation at the International Conference on Basic Sciences, Engineering and Technology (www.icbaset.net) held in Alanya/Turkey on May 02-05, 2024.

References

Bandhu, A., Sutradhar, S., Mukherjee, S., Greneche, J.M., & Chakrabarti, P. K. (2015). Synthesis, characterization and magnetic property of maghemite (γ-Fe_2O_3) nanoparticles and their protective coating with pepsin for bio-functionalization. *Materials Research Bulletin, 70,* 145–154.

Behera, B. Pradhan, S., Samantaray, A., & Pradhan, D. (2020) Antiproliferative and cytotoxic activity of Hematite (α-Fe2O3) nanoparticles from Butea monosperma on MCF-7 cells. *African Journal of Pharmacy and Pharmacology*. *14,* 29–40.

Bhavani, P., Rajababu, C., Arif, M., Reddy, I.V.S., & Reddy, N.R. (2017). Synthesis of high saturation magnetic iron oxide nanomaterials via low temperature hydrothermal method. *Journal of Magnetism and Magnetic Materials, 426,* 459–466.

Bhuiyan, S.H., Miah, M.Y., Paul, S.C., Das Aka, T., Saha, O., Rahaman, M., Sharif, Habiba, J.I., & Ashaduzzaman O. (2020). Green synthesis of iron oxide nanoparticle using Carica papaya leaf extract: Application for photocatalytic degradation of remazol yellow RR dye and antibacterial activity. *Heliyon, 6*, e04603.

Ghosh, D., Majumder, S., & Sharma, P. (2020) Anticancerous activity of transition metal oxide nanoparticles. in: S.K. Saxena, S.M.P. Khurana (Eds.), *NanoBioMedicine,* 107–137.

Gonzalez-Moragas, L., Yu,S.-M., Murillo-Cremaes, N., Laromaine, A., & Roig, A. (2015). Scale-up synthesis of iron oxide nanoparticles by microwave-assisted thermal decomposition. *Chemical Engineering Journal, 281,* 87–95.

Guardia, P., Batlle-Brugal, B., A Roca,.G. Iglesias, O., Morales, M.D.P., Serna, C., Labarta, A., & Batlle, X. (2007). Surfactant effects in magnetite nanoparticles of controlled size. *Journal of Magnetism and Magnetic Materials, 316*, e756–e759.

Jain, T.K., Morales, M.A., Sahoo, S.K., Leslie-Pelecky,D.L., & Labhasetwar, V. (2005). Iron oxide nanoparticles for sustained delivery of anticancer agents. *Molecular Pharmaceutics, 2,* 194–205.

Javed, R., Zia, M., Naz, S., Aisida, S. O. Ain, N.ul & Ao. Q. (2020). Role of capping agents in the application of nanoparticles in biomedicine and environmental remediation: recent trends and future prospects. *Journal of Nanobiotechnology, 18*, 172.

Katsuki, H., & Komarneni, S. (2003). Role of α-Fe2O3 morphology on the color of red pigment for porcelain. *Journal of the American Ceramic Society, 86,* 183–185.

Kumari, S., Yadav, N., Ghosh, D., Srivastava, C., & Majumder, S. (2018). Role of polyvinyl pyrrolidone as a capping agent in the synthesis of magnetite (Fe3O4) nanoparticles. *Indian Journal of Chemistry A, 57*, 1151–1155.

LaGrow, A.P., Besenhard, M.O., Hodzic, A., Sergides, A., Bogart, L.K. Gavriilidis, A., & Thanh, N.T.K. (2019). Unravelling the growth mechanism of the co-precipitation of iron oxide nanoparticles with the aid of synchrotron X-Ray diffraction in solution. *Nanoscale, 11,* 6620–6628.

Lemine, O.M., Sajieddine, M., Bououdina, M., Msalam, R., Mufti, S., & Alyamani, A. (2010). Rietveld analysis and Mossbauer ¨ spectroscopy studies of nanocrystalline hematite α-Fe_2O_3. *Journal of Alloys and Compounds, 50*(2), 279–282.

Mahmoudi, M., Simchi, A., & Imani, M. (2010). Recent advances in surface engineering of superparamagnetic iron oxide nanoparticles for biomedical applications. *Journal of Iranian Chemical Society, 7*, 1–27.

Mornet, S., Portier, J., & Duguet, E. (2005). A method for synthesis and functionalization of ultrasmall super-paramagnetic covalent carriers based on maghemite and dextran. *Journal of Magnetism and Magnetic Materials, 293*, 127–134.

Okoli, C., Sanchez-Dominguez, M., Boutonnet, M., Järås, S., Civera, C., Solans, C., & Kuttuva,G.R. (2012). Comparison and functionalization study of microemulsion-prepared magnetic ıron oxide nanoparticles. *Langmuir, 28*(22), 8479–8485.

Predescu, A. M., Matei, E., Berbecaru, A. C., Pantilimon, C., Drăgan, C., Vidu, R., Predescu C., & Kuncser V. (2018). Synthesis and characterization of dextran-coated ıron oxide nanoparticles. *Royal Society Open Science, 5,* 171525.

Ramasami, P., Baabu S., Kumar, H. K., Gumpu, M. B., J. Babu, K, Kulandaisamy, A. J., & Rayappan, J. B. B. (2023). Iron oxide nanoparticles: a review on the province of ıts compounds, properties and biological applications. *Materials*, *16*(1), 59.

Rasheed, R.T., Al-Algawi, S.D., Kareem, H.H., & Mansoor, H.S. (2018). Preparation and characterization of hematite ıron oxide (α-Fe_2O_3) by sol-gel method. *Chemical Sciences Journal, 9*(4), 1000197.

Ravikumar, C., & Bandyopadhyaya, R. (2011). Mechanistic study on magnetite nanoparticle formation by thermal decomposition and coprecipitation routes. *The Journal of Physical Chemistry C*, *115* (5), 1380–1387.

Sharma, P., Dhiman,S., Kumari, S., Rawat, P., Srivastava, C., Sato, H., Akitsu, T., Kumar, S., Hassan, I., & Majumder, S. (2019). Revisiting the physiochemical properties of Hematite (α-Fe2O3) nanoparticle and exploring its bio-environmental application. *Materials Research Express*, *6*(9), 095072.

Sharma, P., Kumari, S., Ghosh, D., Yadav, V., Vij, A., Rawat, P., Kumar, S., Sinha, C., Saini, S., Sharma, V., Hassan, M. I., Srivastava, C. M., & Majumder, S. (2021). Capping agent-induced variation of physicochemical and biological properties of α-Fe_2O_3 nanoparticles. *Materials Chemistry and Physics*, *258*, 123899,

Tedeschi, L., & Enders, D. (2001). Asymmetric synthesis of β-phosphono malonates via Fe2O3- mediated phospha-michael addition to knoevenagel acceptors. *Organic Letters, 3*, 3515–3517.

Wang, L., Li, Z., Mao, G., Zhang, Y., & Lai, F. P. (2022). Effect of nanoparticle adsorption on the pore structure of a coalbed methane reservoir: A Laboratory Experimental Study. *ACS Omega, 7,* 6261−6270,

Woo, K., Lee, H.J., Ahn, J.P., & Park, Y.S (2003). Sol–gel mediated synthesis of Fe_2O_3 nanorods. *Advanced Materials, 15,* 1761–1764.

Author Information

Gulten Sadullahoglu
Mechatronics Engineering Department, Istanbul Health and Technology University, Türkiye
Contact e-mail: *gulten.sadullahoglu@istun.edu.tr*

To cite this article:

Sadullahoğlu, G. (2024). Optimization of properties of iron oxide nanoparticles synthized by Sol-Gel method. *The Eurasia Proceedings of Science, Technology, Engineering & Mathematics (EPSTEM), 28,* 565-574.